A Steerable Deep Network for Model-Free Diffusion MRI Registration

Gianfranco Cortés[1], Xiaoda Qu[2], and Baba C. Vemuri[1]

[1] Department of CISE, University of Florida, Gainesville, FL, USA
{gcortes, vemuri}@ufl.edu
[2] Department of Statistics, University of Florida, Gainesville, FL, USA
quxiaoda@ufl.edu

Abstract. Nonrigid registration is vital to medical image analysis but remains challenging for diffusion MRI (dMRI) due to its high-dimensional, orientation-dependent nature. While classical methods are accurate, they are computationally demanding, and deep neural networks, though efficient, have been underexplored for nonrigid dMRI registration compared to structural imaging. We present a novel, deep learning framework for model-free, nonrigid registration of raw diffusion MRI data that does not require explicit reorientation. Unlike previous methods relying on derived representations such as diffusion tensors or fiber orientation distribution functions, in our approach, we formulate the registration as an equivariant diffeomorphism of position-and-orientation space. Central to our method is an $\mathsf{SE}(3)$-equivariant UNet that generates velocity fields while preserving the geometric properties of a raw dMRI's domain. We introduce a new loss function based on the maximum mean discrepancy in Fourier space, implicitly matching ensemble average propagators across images. Experimental results on Human Connectome Project dMRI data demonstrate competitive performance compared to state-of-the-art approaches, with the added advantage of bypassing the overhead for estimating derived representations. This work establishes a foundation for data-driven, geometry-aware dMRI registration directly in the acquisition space.

Keywords: Diffusion MRI · Steerable CNN · Special Euclidean Group · Nonrigid Registration · RKHS

1 Introduction

Computing a nonrigid deformation mapping one image, S_m, to another, S_f, is an essential task in medical image analyses, most notably for cross-subject comparisons, population-specific atlas construction, and atlas-based segmentation. This task, known as image registration, possesses well-established classical [12,44,2,43,27] and deep learning [3,14,15] solutions that are readily applicable to 3D scalar-valued modalities of the form $\mathbf{R}^3 \to \mathbf{R}$, such as structural magnetic resonance imaging (sMRI) and computed tomography (CT). However, registration of diffusion MRI (dMRI), an imaging modality primarily used to probe neural microstructure, requires additional care.

Within each voxel, diffusion-weighted imaging captures the diffusion profile of water molecules, which is naturally constrained (or not) by the surrounding tissue. The diffusion profile at a position $\mathbf{p} \in \mathbf{R}^3$ is characterized by the ensemble average propagator (EAP), which is a probability density $\mathsf{P}_{\mathbf{p}}(\mathbf{r}) : \mathbf{R}^3 \to \mathbf{R}_{\geq 0}$ describing the probability of a water molecule being displaced by $\mathbf{r}$ within the effective diffusion time. Practitioners ultimately care about resolving the dominant directions of diffusion at each voxel in order to perform downstream analysis like tractography [28,21,10]. As a means to this end, assumptions are imposed on the unknown EAP (e.g. Gaussian) in order to fit a simplified model (e.g. a diffusion tensor) to the raw signal, with the hope that the principal directions of diffusion are accurately captured. We refer to such models as *derived representations*, examples of which include diffusion tensors (DTs) [4,45,41], fiber orientation distribution functions (fODFs) [39,38,24], orientation distribution functions [55,16], Gaussian mixtures [25], and Hermite basis functions [30].

It follows that diffusion-weighted images and their derived representations carry orientation-dependent information at each voxel that must be properly transformed (i.e. reoriented) under a spatial deformation $\Phi : \mathbf{R}^3 \to \mathbf{R}^3$. While the details of how this reorientation is carried out will depend on the derived representation and domain-specific assumptions (e.g. finite strain), it is always grounded in the fact that if $\mathbf{p}$ is displaced to $\Phi(\mathbf{p})$, then $S_m(\mathbf{p})$ is transformed according to some action of the Jacobian $\mathrm{d}\Phi_{\mathbf{p}}$. The literature is filled with approaches to register both raw dMRI [18,53] and derived representations [1,52,11,33,32] that extend the scalar-valued setting to include this required reorientation step. These methods adhere to the classical image registration formulation where a pair of images is iteratively aligned by minimizing a dissimilarity, as opposed to methods that exploit deep learning.

While various deep learning methodologies [50,3,14,15] have been developed to speedily handle the 3D, scalar-valued registration problem at a fraction of classical runtimes, we are only aware of two data-driven frameworks [51,6] that are designed to address the diffusion-weighted setting. Both of these methods rely on VoxelMorph (VM)-inspired [3] backbones consisting of a UNet [35] that estimates a nonlinear deformation Φ and a spatial transformer [22] that applies Φ to the moving image S_m and handles reorientation. The key distinction between them is their choice of input features. The first of these, DDMReg [51], requires a fractional anisotropy (FA) map and tract orientation maps (TOMs) for each diffusion-weighted image. Note that since these are scalar- and vector-valued features, respectively, they can be fed to a vanilla VM backbone as is. On the other hand, the method of [6], which we will refer to as MVCReg, requires square root density parameterized fODF maps as input. Since these are manifold-valued derived representations, the authors are forced to replace the VM backbone's vanilla convolutions with manifold-valued convolutions [9,5].

In this work, we demonstrate that data-driven registration should and can be performed on the raw dMRI data. Thus our approach is "model-free" in this sense. To facilitate the discussion, we refer to the scalar-valued setting as the anat-$\mathbf{p}$ registration problem, and its aforementioned extension to the diffusion-

Type	anat-**p**	diff-**p**	diff-**pq**
Modalities	sMRI, CT, FA	DT, fODF, GMM	raw dMRI
Driving Mechanism	position	position	position orientation
Registration Schematic	$\mathbf{R}^3 \xrightarrow{S_f} \mathbf{R}$ $\Phi \uparrow\downarrow$ $\mathbf{R}^3 \xrightarrow{S_m} \mathbf{R}$	$\mathbf{R}^3 \xrightarrow{S_f} (\mathbf{R}^3 \to \mathbf{R})$ $\Phi \uparrow\downarrow$ reorient $\updownarrow$ $\mathbf{R}^3 \xrightarrow{S_m} (\mathbf{R}^3 \to \mathbf{R})$	$\mathbf{R}^3 \oplus \mathbf{R}^3 \xrightarrow{S_f} \mathbf{R}$ $\Phi \uparrow\downarrow$ $\mathbf{R}^3 \oplus \mathbf{R}^3 \xrightarrow{S_m} \mathbf{R}$

Fig. 1. Comparison of three registration scenarios in which we try to estimate a deformation Φ that minimizes $\mathcal{L}(S_f, S_m \circ \Phi)$ for some dissimilarity $\mathcal{L}$.

weighted regime as the diff-**p** registration problem (see Fig. 1). Although derived representations offer the conceptual benefit of offloading the orientational information to the codomain, we argue that their usage in registration suffers from two pitfalls: (1) inherent limitations of the model chosen to approximate the acquired data manifest themselves as lost information and (2) the orientational information is not directly leveraged to drive the registration. This second point motivates our formulation of the diff-**pq** registration problem, in which the orientational information is pulled back into the domain, thus allowing the deformation Φ to be a function of both position and orientation (see Fig. 1).

This change in perspective demands that we borrow tools from the field of geometric deep learning (GDL) [7,48], with the aim of generating deformations Φ that respect the geometry of the newly introduced non-Euclidean domain. *We introduce several novel contributions including* (1) the diff-**pq** registration problem and its formalization, which in particular avoids explicit Jacobian estimation and reorientation, (2) an $\mathsf{SE}(3)$-equivariant, end-to-end, VM-inspired network capable of preserving the geometry of a raw diffusion-weighted signal's domain, (3) use of maximum mean discrepancy (MMD) [36] in the Fourier space as a loss function for dMRI registration, and (4) an experimental evaluation on HCP dMRI scans comparing our method to SOTA dMRI registration approaches.

The rest of the paper is organized as follows: In Section 2, we briefly present group-theoretic prerequisites before delving into the theoretical underpinnings of our proposed registration framework. In Section 3, we present the construction of the $\mathsf{SE}(3)$-equivariant convolution layers and our VM-inspired architecture. Section 4 contains experimental results and conclusions are drawn in Section 5.

2 Background

2.1 Representations and Equivariance

Definition 1. *An action of a group G on a space M is a mapping $(g, p) \mapsto g \blacktriangleright p$ satisfying the following properties for all $g, g' \in G$ and $p \in M$: (1) $e \blacktriangleright p = p$ where e is the group identity and (2) $g \blacktriangleright (g' \blacktriangleright p) = (gg') \blacktriangleright p$.*

Definition 2. *A d-dimensional representation of a group G is a map $\rho : G \to$ $\mathsf{GL}(d)$ that satisfies $\rho(gg') = \rho(g)\rho(g')$ for all $g, g' \in G$.*

Definition 3. *Let M and N be spaces with a group G acting on each of them. A function $\Psi : M \to N$ is equivariant to G if $\Psi(g \blacktriangleright_M p) = g \blacktriangleright_N \Psi(p)$ for all $g \in G$ and $p \in M$.*

2.2   The Geometry of Diffusion-Weighted Images

To a first approximation, a diffusion-weighted acquisition sequence can be described as follows: first, select a finite number of directions $\mathbf{g}_j \in \mathbf{S}^2 \subset \mathbf{R}^3$ along which diffusion-sensitized magnetic field gradients are applied; second, acquire a 3D volume for each $\mathbf{g}_j$. At first glance, this would suggest that a raw dMRI is a function $S : \mathbf{R}^3 \times \mathbf{S}^2 \to \mathbf{R}$, since there is a 3D volume $S(-, \mathbf{g}) : \mathbf{R}^3 \to \mathbf{R}$ for every direction $\mathbf{g} \in \mathbf{S}^2$. However, there are two additional idiosyncrasies of a diffusion-weighted acquisition sequence that need to be introduced:

a) For a fixed direction $\mathbf{g}$, we can scale the strength of the applied diffusion-sensitized magnetic field gradient, where the strength is proportional to (the square root of) the so-called b-value. An important and required special case is when $b = 0$.
b) For a fixed b-value, a dMRI exhibits antipodal symmetry, i.e. the 3D volume acquired along $\mathbf{g}$ is equal to the 3D volume acquired along $-\mathbf{g}$.

By (a), there exists a "shell" of directions for each b-value $b \geq 0$ (where $b = 0$ corresponds to a degenerate shell), meaning we should augment our domain to

$$\underbrace{\mathbf{R}^3 \times (\mathbf{S}^2 \times \mathbf{R}_+)}_{b>0} \cup \underbrace{(\mathbf{R}^3 \times \{0\})}_{b=0} \simeq \mathbf{R}^3 \times \mathbf{R}^3. \tag{1}$$

By (b), a dMRI $S : \mathbf{R}^3 \times \mathbf{R}^3 \to \mathbf{R}$ must satisfy

$$S(\mathbf{p}, \mathbf{q}) = S(\mathbf{p}, -\mathbf{q}) \text{ for all } \mathbf{p}, \mathbf{q} \in \mathbf{R}^3. \tag{2}$$

This constraint is equivalent to saying that f is a function

$$\mathbf{R}^3 \times (\mathbf{RP}^2 \times \mathbf{R}_+) \cup (\mathbf{R}^3 \times \{0\}) \to \mathbf{R}, \tag{3}$$

where $\mathbf{RP}^2$ is the real projective plane obtained by identifying antipodes on S^2. Nevertheless, for notational convenience, we will think of a dMRI as a function

$$\underbrace{\mathbf{R}^3}_{\mathbf{p}\text{-space}} \times \underbrace{\mathbf{R}^3}_{\mathbf{q}\text{-space}} \to \mathbf{R} \tag{4}$$

satisfying Eqn. 2, where we deliberately split the domain into $\mathbf{p}$-space and $\mathbf{q}$-space. The reasoning for this is twofold. From an acquisition perspective, $\mathbf{p}$-space and $\mathbf{q}$-space are sampled differently, with $\mathbf{p}$-space being sampled on a fixed, uniform Cartesian grid and $\mathbf{q}$-space being sampled at $\mathbf{q} = \mathbf{0}$ and on approximately

uniform spherical grids corresponding to a small number of selected b-values. This is called a multi-shell acquisition, and a single-shell acquisition is the special case where the signal is only sampled at one nonzero b-value. From a geometric perspective, Eqns. 2 and 4 are still not enough to fully characterize the diffusion-weighted signal, because $\mathbf{R}^3 \times \mathbf{R}^3 \cong \mathbf{R}^6$ only describes the domain *as a set*. In fact, $\mathbf{p}$-space and $\mathbf{q}$-space are physically coupled in a manner that can only be captured by an action (see Def. 1) of $\mathsf{SE}(3) = \mathbf{R}^3 \rtimes \mathsf{SO}(3)$, the group of 3D roto-translations. This action is given by

$$(t, r) \blacktriangleright (\mathbf{p}, \mathbf{q}) = (r\mathbf{p} + t, r\mathbf{q}) \tag{5}$$

for all $(t, r) \in \mathsf{SE}(3)$ and $(\mathbf{p}, \mathbf{q}) \in \mathbf{R}^3 \times \mathbf{R}^3$. This entails that any dMRI S must appropriately transform under a roto-translation of the domain, i.e.

$$[(t, r) \blacktriangleright S](\mathbf{p}, \mathbf{q}) = S(r^{-1}(\mathbf{p} - t), r^{-1}\mathbf{p}). \tag{6}$$

To prevent ourselves from viewing the domain $\mathbf{R}^3 \times \mathbf{R}^3$ as just a set in isolation, we will follow [29] in using the notation $\mathbf{R}^3 \oplus \mathbf{R}^3$ as a reminder that $\mathbf{p}$-space and $\mathbf{q}$-space are coupled in a manner less trivial than a direct product.

2.3 The diff-$\mathbf{pq}$ Registration Problem

We demonstrated in Section 2.2 that the natural domain for a raw diffusion-weighted signal is $\mathbf{R}^3 \oplus \mathbf{R}^3$, where the first factor denotes $\mathbf{p}$-space and the second factor denotes $\mathbf{q}$-space. In the case of a derived representation, the $\mathbf{q}$-space is usually offloaded to the codomain, forcing us to formulate the deformation of one derived representation into another (of same type) as a diff-$\mathbf{p}$ registration problem. However, much akin to the anat-$\mathbf{p}$ registration problem, we are now dealing with scalar-valued functions whose alignment is simply a matter of reparameterizing the domain via an appropriate diffeomorphism Φ. Hence, this naturally gives way to the diff-$\mathbf{pq}$ registration problem, which we state here for completeness: Given raw diffusion-weighted signals $S_m, S_f : \mathbf{R}^3 \oplus \mathbf{R}^3 \to \mathbf{R}$, estimate a diffeomorphism $\Phi : \mathbf{R}^3 \oplus \mathbf{R}^3 \to \mathbf{R}^3 \oplus \mathbf{R}^3$ that minimizes $\mathcal{L}(S_f, S_m \circ \Phi)$ for some dissimilarity $\mathcal{L}$.

Notice that the notation $\mathbf{R}^3 \oplus \mathbf{R}^3$ carries weight in this setting, because a diffeomorphism $\mathbf{R}^3 \oplus \mathbf{R}^3 \to \mathbf{R}^3 \oplus \mathbf{R}^3$ is *not* the same as a diffeomorphism $\mathbf{R}^3 \times \mathbf{R}^3 \to \mathbf{R}^3 \times \mathbf{R}^3$. In particular, a diffeomorphism $\Phi : \mathbf{R}^3 \oplus \mathbf{R}^3 \to \mathbf{R}^3 \oplus \mathbf{R}^3$ must commute with the $\mathsf{SE}(3)$ group action in Eqn. 6, a condition that is best visualized with the following commutative diagram:

$$\begin{array}{ccc}
\mathbf{R}^3 \oplus \mathbf{R}^3 & \xrightarrow{\ \Phi\ } & \mathbf{R}^3 \oplus \mathbf{R}^3 \\
{\scriptstyle (t,r)\blacktriangleright}\big\downarrow & & \big\downarrow{\scriptstyle (t,r)\blacktriangleright} \\
\mathbf{R}^3 \oplus \mathbf{R}^3 & \xrightarrow{\ \Phi\ } & \mathbf{R}^3 \oplus \mathbf{R}^3
\end{array} \tag{7}$$

The commutative diagram in Eqn. 7 is saying that both paths from the top-left corner to the bottom-right corner are equivalent. Such a Φ is called an *equivariant*

diffeomorphism. Therefore, we require some kind of sufficient condition that will guarantee that we can construct equivariant diffeomorphisms, which will ensure that we do not violate the physical coupling of **p**- and **q**-space. Fortunately, we can accomplish this by invoking the following theorem [46]:

Theorem 1. *[46] Let M be a Riemannian manifold with a Lie group G acting on it. Let X be an equivariant vector field on M, i.e. $X_{gp} = gX_p$ for all $p \in M$ and $g \in G$. Then, the flow generated by X is an equivariant diffeomorphism.*

Hence, it is sufficient for us to generate an equivariant vector (velocity) field, which we may then integrate to obtain an equivariant diffeomorphism.

Before proceeding, we remind the reader that, in practice, **q**-space is sampled on a small number of concentric spherical shells. Therefore, although the diffusion-weighted signal does exist on all of $\mathbf{R}^3 \oplus \mathbf{R}^3$, it is more prudent to refine our treatment to the constituent shells and piece them back together when needed. When we restrict ourselves to a single shell we will call the new domain Ω, which is $\mathbf{R}^3 \times \mathbf{S}^2$ as a set (cf. Eqn. 1). The $\mathsf{SE}(3)$ group action (Eqn. 5) is exactly the same as before, just restricted to this subspace.

2.4 Steerable Convolutions

Using convolutions to generate an equivariant velocity field on Ω imposes two conditions on the convolutions themselves: (1) the convolutions must be $\mathsf{SE}(3)$-equivariant and (2) the convolutions must be able to *output vector fields* on Ω. Although $\mathsf{SE}(3)$-equivariant layers were developed in [26] to handle raw dMRI signals, their method relies on the regular group representation which is *incapable of producing vector fields*. Instead, we need to extend the steerable convolutions introduced in [13,8], otherwise known as gauge equivariant convolutions, to the domain Ω. We now give a brief primer on steerability; see [48] for more detail.

Let M be a 5-dimensional Riemannian manifold with structure group $\mathsf{SO}(5)$, the group of 5D rotations. In the steerable setting, feature maps become tensor fields on M (e.g. vector – order one tensor – fields). A feature map is coordinatized w.r.t. a gauge, a local choice of coordinate frame. A steerable convolution maps an input feature map f_{in} of type ρ_{in} to an output feature map f_{out} of type ρ_{out}, where ρ_{in} and ρ_{out} are group representations that encode the transformation behavior of the tensor components under a change of gauge [48]. Let f_{in} be a feature map of type ρ_{in} and $K : \mathbf{R}^5 \to \mathbf{R}^{d_{\mathrm{out}} \times d_{\mathrm{in}}}$ a matrix-valued filter where d_{in} and d_{out} are the dimensions of the input and output tensors, respectively. Letting $q_v := \exp_p w_p v$ (exp denotes the Riemannian exponential map and $w_p : \mathbf{R}^5 \to T_p M$ a gauge), the convolved feature map $f_{\mathrm{out}} = K \star f_{\mathrm{in}}$ is given pointwise w.r.t. w_p by

$$f_{\mathrm{out}}(p) := \int_{\mathbf{R}^5} K(v)\rho_{\mathrm{in}}(t_{p \leftarrow q_v})f_{\mathrm{in}}(q_v)\, dv, \tag{8}$$

where $t_{p \leftarrow q_v}$ denotes the $\mathsf{SO}(5)$-valued gauge transformation taking the frame on q_v (after parallel transportstion to p) to the frame on p. Eqn. 8 is equivariant

to a change of gauge at p if and only if K is $\mathsf{SO}(5)$-*steerable*, i.e. K satisfies

$$K(t^{-1}v) = \rho_{\text{out}}(t^{-1})K(v)\rho_{\text{in}}(t) \tag{9}$$

for all $t \in \mathsf{SO}(5)$ and $v \in \mathbf{R}^5$ [13]. A critical result of [48] shows that, in the case where $M = \Omega$, steerable convolutions with $\mathsf{SO}(5)$-steerable filters are equivariant to 3D rototranslations.

2.5 An MMD Loss via Characteristic Functions

We argue that the ultimate goal of raw dMRI registration is not merely to align the raw signals S_f and S_m, but rather to match their corresponding EAPs. As we shall see in Section 4, this claim is evidenced by the fact that registration quality in the dMRI setting is evaluated using white matter fiber bundle segmentations, which are extracted using fODF peaks (an approximation of EAP peaks). The relation between the raw signal S and its associated EAP, P, is given by

$$\mathsf{P}_{\mathbf{p}}(\mathbf{r}) = \int_{\mathbf{R}^3} e^{2\pi i \mathbf{q}^\top \mathbf{r}} E(\mathbf{p}, \mathbf{q}) \, \mathrm{d}\mathbf{q}, \tag{10}$$

where $E(\mathbf{p}, \mathbf{q}) = S(\mathbf{p}, \mathbf{q})/S(\mathbf{p}, \mathbf{0})$ is the signal attenuation. Therefore, if every diffusion-weighted volume is normalized by the $b = 0$ volume, the resulting E is directly related to the EAP via a Fourier transform. Said differently, for every position $\mathbf{p}$, $E(\mathbf{p}, -)$ is the characteristic function of the probability density $\mathsf{P}_{\mathbf{p}}$. We now introduce a result from the theory of reproducing kernel Hilbert spaces (RKHSs) that permits us to indirectly minimize the maximum mean discrepancy (MMD) between EAPs via a modified L^2 loss applied to the signal attenuations.

Suppose P and Q are two distributions on $\mathbf{R}^3$ with corresponding characteristic functions (Fourier transforms) ϕ_P and ϕ_Q respectively, and let k be a kernel function on $\mathbf{R}^3$, associated with the RKHS $\mathcal{H}_k$. The MMD between P and Q is defined as

$$\mathrm{MMD}(P, Q) = \sup_{f \in \mathcal{H}_k, \|f\| \leq 1} \left| \int_{\mathbf{R}^3} f \, \mathrm{d}P - \int_{\mathbf{R}^3} f \, \mathrm{d}Q \right|. \tag{11}$$

Bochner's theorem [36, Thm. 3] states that there exists a finite Borel measure Λ on $\mathbf{R}^3$ such that

$$k(\mathbf{r}, \mathbf{r}') = \int_{\mathbf{R}^3} e^{-i(\mathbf{r}-\mathbf{r}')^\top \mathbf{q}} \, \mathrm{d}\Lambda(\mathbf{q}). \tag{12}$$

It was shown in [36] that

$$\mathrm{MMD}(P, Q) = \|\phi_P - \phi_Q\|_{L^2(\mathbf{R}^3, \Lambda)}, \tag{13}$$

i.e. the MMD between P and Q equals the L^2 distance between their *characteristic functions* with respect to the measure Λ. In this work, we choose Λ to be the multivariate Gaussian distribution (measure) $N(\mathbf{0}, \sigma^2 I_3)$, whose corresponding kernel k is exactly the Gaussian kernel $k(\mathbf{r}, \mathbf{r}') = \exp(-\frac{\sigma^2}{2}\|\mathbf{r} - \mathbf{r}'\|^2)$. In this case, the L^2 loss between P and Q equals

$$\mathrm{MMD}(P, Q) = \mathbf{E}|\phi_P(X) - \phi_Q(X)|^2, \quad X \sim N(\mathbf{0}, \sigma^2 I_3). \tag{14}$$

Letting $\mathcal{E}(\mathbf{p}, \mathbf{q}) := |E_f(\mathbf{p}, \mathbf{q}) - [E_m \circ \Phi](\mathbf{p}, \mathbf{q})|^2$, this translates to the following loss in our setting:

$$\mathcal{L}(E_f, E_m \circ \Phi) = C \sum_{\mathbf{p}, \mathbf{q}} \mathcal{E}(\mathbf{p}, \mathbf{q}) \cdot e^{-\|\mathbf{q}\|^2/2\sigma^2} \cdot \|\mathbf{q}\|^2 + \lambda \sum_{\mathbf{p}, \mathbf{q}} \|v(\mathbf{p}, \mathbf{q})\|^2. \quad (15)$$

Here, λ is the regularization hyperparameter, v is the velocity field generated by the UNet described in Section 3, and $C = (2\pi\sigma^2)^{-\frac{3}{2}}$ is a normalization constant. Note that the guarantee provided by Eqn. 13 would not hold if we simply resorted to a standard MSE loss, since a Lebesgue measure in isolation is not finite.

3   Implementation

3.1   Constructing SE(3)-Equivariant Convolution Layers

The most challenging obstacle to implementing the steerable convolutions of Section 2.4 in practice is generating an SO(5)-steerable filter that satisfies Eqn. 9. Historically, this is done in one of two ways: (1) analytically solve for a basis of the linear subspace of filters satisfying Eqn. 9, or (2) parameterize the convolution filter using an equivariant MLP. We opt for the second approach since it circumvents the need to solve for an explicit basis, and it has shown superior performance in equivariant tasks [54]. We can invoke the following lemma to parameterize a filter that satisfies Eqn. 9 using an MLP:

Lemma 1. *[54] If a filter K is parameterized by an SO(5)-equivariant MLP with input representation ρ_{st} and output representation $\rho_\otimes := \rho_{in} \otimes \rho_{out}$, then the filter satisfies the steerability constraint in Equation 9.*

In Lemma 1 above, ρ_{st} denotes the standard representation given by $\rho_{st}(g) = g$ and $\rho_\otimes$ denotes the tensor product representation given by $\rho_\otimes(g) = \rho_{in}(g) \otimes \rho_{out}(g)$. We can construct an SO(5)-equivariant MLP matching the description of Lemma 1 by using the open source method of [19]. To summarize briefly, the authors of [19] efficiently build equivariant MLPs by decomposing the equivariance constraint into a finite set of simpler constraints involving the Lie group's generators, which are elements of its Lie algebra. These constraints can be solved efficiently at initialization time, and are thus a one-time computational cost.

3.2   Network Input

To prevent wasting model capacity on learning large, parameterizable motion between images, we follow the preparatory step of affinely aligning a moving image to the fixed image, as suggested in [6]. This is important for two reasons. Firstly, nonlinear registration algorithms generally require a sensible initialization to perform well. Secondly, since VM-inspired registration makes the implicit assumption that the moving and fixed images are roughly aligned in $\mathbf{p}$-space before concatenation, we need to ensure that this assumption is also met in $\mathbf{q}$-space so that concatenation remains meaningful. Therefore, we take advantage of the

affine pre-alignment step to also resample the moving image's $\mathbf{q}$-space at the fixed image's $\mathbf{q}$-vectors. The framework of [37,18] permits us to perform both tasks in one step using angular interpolation (see Eqn. 19).

As motivated in Section 2.5, we then normalize the diffusion-weighted volumes by the mean $b = 0$ volume, and thus we now call the moving and fixed images E_m and E_f, respectively. Finally, to address noise in the raw signal attenuations, we apply a low-pass filter to the training data. For a fixed voxel, the intensities on a given shell are expanded in terms of a truncated spherical harmonic basis ($\ell_{\max} = 5$). This yields $\sum_{\ell=0}^{\ell_{\max}}(2\ell+1)$ coefficients per shell. These coefficients are then smoothed spatially across voxels using a Gaussian filter. The signal attenuations are subsequently reconstructed from the smoothed spherical harmonic coefficients, yielding a denoised representation suitable for training.

3.3   Network Architecture

In the spirit of DDMReg [51] and MVCReg [6], we continue the successful trend of using a VM-inspired backbone to perform image registration, while also incorporating the crucial property of $\mathsf{SE}(3)$-equivariance. The first module is the UNet, which is responsible for generating a velocity field v on the domain Ω. Our UNet has an encoder depth of 3. Each layer consists of an $\mathsf{SE}(3)$-equivariant convolution as described in Sections 2.4 and 3.1, followed by swish nonlinearities [34] on scalar features and gated nonlinearities [49] on higher order features, followed by e3nn-inspired batch normalization [20]. We interleave the encoding layers with average pooling across $\mathbf{p}$-space.

Next, inspired by [14], a scaling-and-squaring layer integrates the velocity field v to apply a diffeomorphism Φ. We relate v to Φ via the differential equation

$$\frac{\mathrm{d}\Phi^{(t)}}{\mathrm{d}t} = v(\Phi^{(t)}), \;\; \Phi^{(0)} = \mathrm{id} \tag{16}$$

by stipulating that $\Phi = \Phi^{(1)}$. Hence, $\Phi = \exp(v)$, and scaling-and-squaring is a numerical technique that approximates this exponential map. This is done by first scaling v by 2^{-N} to create an incrementally small displacement $\Phi^{(0)}(\mathbf{p}, \mathbf{g}) = \exp(2^{-N}v(\mathbf{p}, \mathbf{g}))$. Recall $(\mathbf{p}, \mathbf{g}) \in \Omega$ (see Section 2.2). Then, the displacement is squared iteratively N times:

$$\Phi^{(j+1)}(\mathbf{p}, \mathbf{g}) = \Phi^{(j)}(\Phi^{(j)}(\mathbf{p}, \mathbf{g})), \;\; j = 0, 1, \ldots, N-1. \tag{17}$$

After N squaring steps, $\Phi^{(N)}(\mathbf{p}, \mathbf{g})$ approximates $\Phi(\mathbf{p}, \mathbf{g}) = \exp(v(\mathbf{p}, \mathbf{g}))$. We set $N = 4$ in our implementation. We represent a tangent vector $v(\mathbf{p}, \mathbf{g})$ as a 6D vector whose first three components are the tangent vector $v_{\mathbf{R}^3}$ and whose last three components are the tangent vector $v_{\mathbf{S}^2}$ (embedded in $\mathbf{R}^3$). Using this representation, we have that

$$\exp(v(\mathbf{p}, \mathbf{g})) = \left(\mathbf{p} + v_{\mathbf{R}^3}, \cos(||v_{\mathbf{S}^2}||)\mathbf{g} + \sin(||v_{\mathbf{S}^2}||)\frac{v_{\mathbf{S}^2}}{||v_{\mathbf{S}^2}||} \right). \tag{18}$$
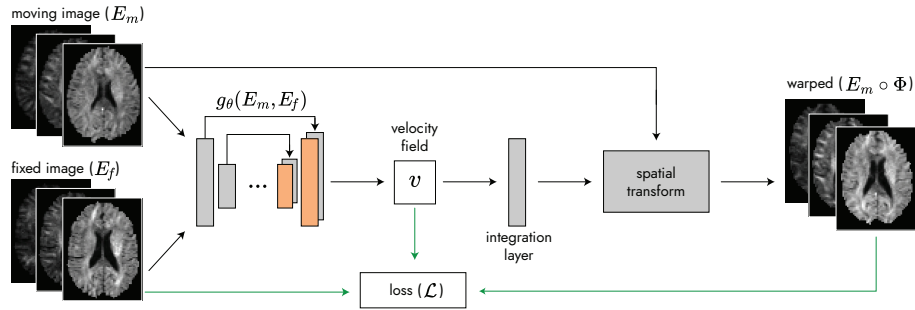
Fig. 2. Overview of the proposed registration pipeline, parameterized by an SE(3)-equivariant UNet g_θ.

Finally, a spatial transformer module tailored to the manifold Ω applies the computed displacement Φ to the moving image E_m, yielding the warped image. This is done by using trilinear interpolation in **p**-space and angular interpolation in **q**-space [37]. Given the signal attenuation E sampled at orientations $\mathbf{g}_j$, we interpolate the attenuation value at $(\mathbf{p}, \mathbf{g}) \in \Omega$ as

$$E(\mathbf{p}, \mathbf{g}) = \frac{\sum_j w_j E(\mathbf{p}, \mathbf{g}_j)}{\sum_j w_j}, \quad w^j = e^{-(\arccos(|\mathbf{g}^\top \mathbf{g}_j|))^2/2\sigma^2} \tag{19}$$

where each w_j is a spherical radial basis function (RBF) centered at $\mathbf{g}_j$ with Gaussian kernel and smoothness parameter σ. The absolute value comes from Eqn. 2. We set $\sigma = 0.1$ in our implementation. See Figure 2 for a schematic of our network architecture.

4   Experiments

4.1   dMRI Registration Applied to HCP Data

Dataset We conducted training and evaluation using minimally preprocessed dMRI data from the Human Connectome Project (HCP) Young Adult dataset. This dataset contains dMRI brain scans from 1,200 individuals aged 22–35. Detailed information about the acquisition parameters, subject selection criteria, and preprocessing steps can be found in the original HCP study [42]. For our analysis, we selected the same 400 subjects as in MVCReg to facilitate a more direct performance comparison. Using MRtrix3 [40], 51 (25 validation subjects, 25 testing subjects, and 1 fixed subject) of these subjects underwent three-tissue response function estimation [17] and multi-shell multi-tissue constrained spherical deconvolution [23] to yield fODF maps. These were subsequently intensity normalized and bias field corrected [31] before finally extracting the fODF peaks, which are needed for model evaluation.

Table 1. Test time performance of various registration methods, average over all 25 test subjects and all 72 available white matter tracts.

Method	Ours	mrregister	VoxelMorph	DDMreg	MVCReg	MVVSReg
Modality	raw dMRI	fODF	FA	FA, TOM	fODF	fODF
Dice	0.7468	0.7601	0.7126	0.7417	0.7317	0.7493

Evaluation We evaluate registration quality by comparing the overlap of known white matter tracts in the warped and fixed image. We measure this overlap using the Dice score. To generate segmentations of white matter tracts, we use the well-validated TractSeg segmentation model [47], which is capable of segmenting 72 distinct white matter tracts. The 51 peak maps produced above serve as input to the TractSeg software. For each of the 25 validation subjects and the fixed subject, we generated tract orientation maps (TOMs) for all 72 bundles. In the diff-**p** setting, validation can be easily performed by applying the estimated deformation $\Phi : \mathbf{R}^3 \to \mathbf{R}^3$ to bundle segmentations of the moving image S_m and measuring the resulting overlap with bundle segmentations of the fixed image S_f. However, in our diff-**pq** setting, it does not immediately make sense to warp a bundle segmentation (a 3D volume) with a deformation $\Omega \to \Omega$. Therefore, we are forced to predict our model's test time behavior by monitoring a different metric, namely the alignment of warped TOMs with the fixed image's TOMs. At test time, the 25 moving test subjects are warped by the model and subsequently fed to TractSeg to generate bundle segmentation masks for all 72 bundles, which are then compared with the fixed subject's bundle segmentation masks.

We selected the same fixed image as in MVCReg [6], and all other subjects are registered to this fixed image. Hence, there are 399 moving/fixed image pairs, 349 of which are used for training, 25 of which are used for validation, and 25 of which are used for testing. Since this task is memory-intensive, we are forced to downsample the spatial dimensions from $145 \times 174 \times 145$ to $72 \times 88 \times 72$.

We trained our model for 500 epochs and we used stochastic gradient descent (SGD) with Nesterov momentum as an optimizer, which we found worked better than Adam on our small batch size of 1. Our initial learning rate was 0.001 and we used a learning rate scheduler that halves the learning rate every 100 epochs.

We compare our method against one classical approach (`mrregister`) and four deep learning approaches (VoxelMorph, DDMReg, MVCReg, MVVSReg). MRtrix3's `mrregister` [33,32] is a classical method based on symmetric normalization (SyN). We also include a VoxelMorph baseline trained on FA maps. Both DDMReg and MVCReg are methods specifically designed for dMRI registration, as discussed in the introduction. MVVSReg [6] is an extension of MVCReg that uses second order, manifold-valued convolutions.

Results Quantitative and qualitative results on HCP dMRI registration are presented in Table 1 and Figure 3, respectively. Figure 3 uses checkerboard masks in parts (d) and (e) to overlay alternating patches from two images, enabling
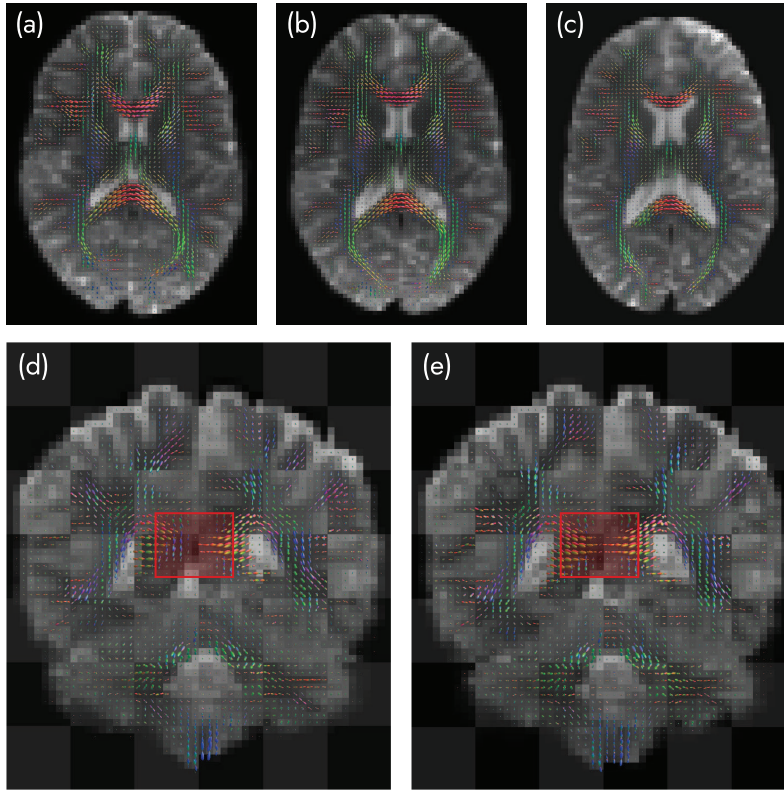
Fig. 3. Visualization of registration results. Top row: $b = 0$ axial slices with overlaid fODF maps. Bottom row: $b = 0$ coronal slices with overlaid fODF maps. (a) Moving source image, (b) warped source image, (c) fixed target image, (d) checkerboard view of moving vs. fixed image, (e) checkerboard view of warped vs. fixed image. The highlighted ROI shows a tract discontinuity in (d) that is resolved after warping in (e). Note that $\mathsf{SE}(3)$-equivariance preserves white matter fiber tracts during warping.

visual assessment of registration quality by highlighting alignment differences between the moving and fixed images (d) or the warped and fixed images (e). Our method outperforms all data-driven, SOTA methods in Dice score except MVVSReg. We attribute this to the fact that MVVSReg utilizes higher order convolutions that capture richer features, though at the expense of higher computation-time/space (memory) complexities [6]. Furthermore, we emphasize that none of the other methods are capable of registering the raw diffusion-weighted data. Hence, they require additional offline overhead to estimate input features. Overall, our method strikes a balance between competitive registration quality and generality, offering a solution to practitioners who do not want to a priori commit to a specific derived representation at this stage of their pipeline.

5   Conclusion

In this paper, we have introduced a novel framework for registering raw dMRI signals that more directly leverages orientational information. We accomplish this by constructing an SE(3)-equivariant UNet to generate velocity fields on the raw signal domain, and by applying key theoretical results to ensure that the physical coupling of **p**- and **q**-space is preserved. To our knowledge, we are the first to present a data-driven technique that registers the raw dMRI signals, as opposed to first computing some derived representation. Our HCP dMRI registration experiment demonstrates that the proposed method achieves competitive performance against state-of-the-art deep learning registration approaches. In future work, we aim to apply our proposed registration method to dMRI scans from patient groups with neurodegenerative disorders.

References

1. Alexander, D.C., Pierpaoli, C., Basser, P.J., Gee, J.C.: Spatial transformations of diffusion tensor magnetic resonance images. IEEE transactions on medical imaging **20**(11), 1131–1139 (2001)
2. Avants, B.B., Epstein, C.L., Grossman, M., Gee, J.C.: Symmetric diffeomorphic image registration with cross-correlation: evaluating automated labeling of elderly and neurodegenerative brain. Medical image analysis **12**(1), 26–41 (2008)
3. Balakrishnan, G., Zhao, A., Sabuncu, M.R., Guttag, J., Dalca, A.V.: Voxelmorph: a learning framework for deformable medical image registration. IEEE transactions on medical imaging **38**(8), 1788–1800 (2019)
4. Basser, P.J., Mattiello, J., Lebihan, D.: Estimation of the effective self-diffusion tensor from the nmr spin echo. Journal of Magnetic Resonance Ser. B **103**(3), 247–254 (1994)
5. Bouza, J.J., Yang, C.H., Vaillancourt, D., Vemuri, B.C.: A higher order manifold-valued convolutional neural network with applications to diffusion mri processing. In: Information Processing in Medical Imaging: 27th International Conference, IPMI 2021, Virtual Event, June 28–June 30, 2021, Proceedings 27. pp. 304–317. Springer (2021)
6. Bouza, J.J., Yang, C.H., Vemuri, B.C.: Geometric deep learning for unsupervised registration of diffusion magnetic resonance images. In: International Conference on Information Processing in Medical Imaging. pp. 563–575. Springer (2023)
7. Bronstein, M.M., Bruna, J., LeCun, Y., Szlam, A., Vandergheynst, P.: Geometric deep learning: going beyond euclidean data. IEEE Signal Processing Magazine **34**(4), 18–42 (2017)
8. Cesa, G., Lang, L., Weiler, M.: A program to build E(N)-equivariant steerable CNNs. In: International Conference on Learning Representations (ICLR) (2022), https://openreview.net/forum?id=WE4qe9xlnQw
9. Chakraborty, R., Bouza, J., Manton, J.H., Vemuri, B.C.: Manifoldnet: A deep neural network for manifold-valued data with applications. IEEE Transactions on Pattern Analysis and Machine Intelligence **44**(2), 799–810 (2020)
10. Cheng, G., Salehian, H., Forder, J., Vemuri, B.C.: Tractography from hardi using an intrinsic unscented kalman filter. IEEE Transactions on Medical Imaging **35**(1), 298–305 (2014)

11. Cheng, G., Vemuri, B.C., Carney, P.R., Mareci, T.H.: Non-rigid registration of high angular resolution diffusion images represented by gaussian mixture fields. In: Medical Image Computing and Computer-Assisted Intervention–MICCAI 2009: 12th International Conference, London, UK, September 20-24, 2009, Proceedings, Part I 12. pp. 190–197. Springer (2009)
12. Christensen, G.E., Rabbitt, R.D., Miller, M.I.: Deformable templates using large deformation kinematics. IEEE transactions on image processing **5**(10), 1435–1447 (1996)
13. Cohen, T., Weiler, M., Kicanaoglu, B., Welling, M.: Gauge equivariant convolutional networks and the icosahedral CNN. In: Proceedings of the 36th International Conference on Machine Learning. Proceedings of Machine Learning Research, vol. 97, pp. 1321–1330. PMLR (09–15 Jun 2019)
14. Dalca, A.V., Balakrishnan, G., Guttag, J., Sabuncu, M.R.: Unsupervised learning of probabilistic diffeomorphic registration for images and surfaces. Medical image analysis **57**, 226–236 (2019)
15. Demir, B., Tian, L., Greer, H., Kwitt, R., Vialard, F.X., Estépar, R.S.J., Bouix, S., Rushmore, R., Ebrahim, E., Niethammer, M.: Multigradicon: A foundation model for multimodal medical image registration. In: International Workshop on Biomedical Image Registration. pp. 3–18. Springer (2024)
16. Descoteaux, M., Deriche, R., Le Bihan, D., Mangin, J.F., Poupon, C.: Multiple q-shell diffusion propagator imaging. Medical Image Analysis **15**(4), 603–621 (2010)
17. Dhollander, T., Raffelt, D., Connelly, A.: Unsupervised 3-tissue response function estimation from single-shell or multi-shell diffusion mr data without a co-registered t1 image. In: ISMRM workshop on breaking the barriers of diffusion MRI. vol. 5. Lisbon, Portugal (2016)
18. Duarte-Carvajalino, J.M., Sapiro, G., Harel, N., Lenglet, C.: A framework for linear and non-linear registration of diffusion-weighted mris using angular interpolation. Frontiers in neuroscience **7**, 41 (2013)
19. Finzi, M., Welling, M., Wilson, A.G.: A practical method for constructing equivariant multilayer perceptrons for arbitrary matrix groups. In: International conference on machine learning. pp. 3318–3328. PMLR (2021)
20. Geiger, M., Smidt, T.: e3nn: Euclidean neural networks. arXiv preprint arXiv:2207.09453 (2022)
21. Hagmann, P., Jonasson, L., Maeder, P., Thiran, J.P., Wedeen, V.J., Meuli, R.: Understanding diffusion mr imaging techniques: from scalar diffusion-weighted imaging to diffusion tensor imaging and beyond. Radiographics **26**(suppl_1), S205–S223 (2006)
22. Jaderberg, M., Simonyan, K., Zisserman, A., et al.: Spatial transformer networks. Advances in neural information processing systems **28** (2015)
23. Jeurissen, B., Tournier, J.D., Dhollander, T., Connelly, A., Sijbers, J.: Multi-tissue constrained spherical deconvolution for improved analysis of multi-shell diffusion mri data. NeuroImage **103**, 411–426 (2014)
24. Jian, B., Vemuri, B.C.: A unified computational framework for deconvolution to reconstruct multiple fibers from diffusion weighted mri. IEEE Trans. on Med. Imaging **26**(11), 1464–1471 (2007)
25. Jian, B., Vemuri, B.C., Özarslan, E., Carney, P.R., Mareci, T.H.: A novel tensor distribution model for the diffusion-weighted mr signal. Neuroimage **37**(1), 164–176 (2007)
26. Liu, R., Lauze, F., et al.: SE(3) Group Conv. NN and a Study on Group Convs. and Equivariance for DWI Segmen-

tation   (2023).   https://doi.org/10.21203/rs.3.rs-2531880/v1, https://europepmc.org/article/PPR/PPR624395, preprint

27. Lorenzi, M., Pennec, X.: Geodesics, parallel transport & one-parameter subgroups for diffeomorphic image registration. International Journal of Computer Vision **105**(2), 111–127 (2013)

28. McGraw, T., Vemuri, B.C., Chen, Y., Rao, M., Mareci, T.: Dt-mri denoising and neuronal fiber tracking. Medical Image Analysis **8**(2), 95–111 (2004)

29. Müller, P., Golkov, V., Tomassini, V., Cremers, D.: Rotation-equivariant deep learning for diffusion mri. arXiv preprint arXiv:2102.06942 (2021)

30. Özarslan, E., Koay, C.G., Shepherd, T.M., Komlosh, M.E., İrfanoğlu, M.O., Pierpaoli, C., Basser, P.J.: Mean apparent propagator (map) mri: a novel diffusion imaging method for mapping tissue microstructure. NeuroImage **78**, 16–32 (2013)

31. Raffelt, D., Dhollander, T., Tournier, J.D., Tabbara, R., Smith, R.E., Pierre, E., Connelly, A.: Bias field correction and intensity normalisation for quantitative analysis of apparent fibre density. In: Proc. Intl. Soc. Mag. Reson. Med. vol. 25, p. 3541 (2017)

32. Raffelt, D., Tournier, J.D., Crozier, S., Connelly, A., Salvado, O.: Reorientation of fiber orientation distributions using apodized point spread functions. Magnetic resonance in medicine **67**(3), 844–855 (2012)

33. Raffelt, D., Tournier, J.D., Fripp, J., Crozier, S., Connelly, A., Salvado, O.: Symmetric diffeomorphic registration of fibre orientation distributions. Neuroimage **56**(3), 1171–1180 (2011)

34. Ramachandran, P., Zoph, B., Le, Q.V.: Searching for activation functions. arXiv preprint arXiv:1710.05941 (2017)

35. Ronneberger, O., Fischer, P., Brox, T.: U-net: Convolutional networks for biomedical image segmentation. In: Medical image computing and computer-assisted intervention–MICCAI 2015: 18th international conference, Munich, Germany, October 5-9, 2015, proceedings, part III 18. pp. 234–241. Springer (2015)

36. Sriperumbudur, B.K., Gretton, A., Fukumizu, K., Schölkopf, B., Lanckriet, G.R.: Hilbert space embeddings and metrics on probability measures. The Journal of Machine Learning Research **11**, 1517–1561 (2010)

37. Tao, X., Miller, J.V.: A method for registering diffusion weighted magnetic resonance images. In: International Conference on Medical Image Computing and Computer-Assisted Intervention. pp. 594–602. Springer (2006)

38. Tournier, D.J., Calamante, F., Connelly, A.: Robust determination of the fibre orientation distribution in diffusion mri: non-negativity constrained super-resolved spherical deconvolution. Neuroimage **35**(4), 1459–1472 (2007)

39. Tournier, J.D., Calamante, F., Gadian, D.G., Connelly, A.: Direct estimation of the fiber orientation density function from diffusion-weighted mri data using spherical deconvolution. Neuroimage **23**(3), 1176–1185 (2004)

40. Tournier, J.D., Smith, R., Raffelt, D., Tabbara, R., Dhollander, T., Pietsch, M., Christiaens, D., Jeurissen, B., Yeh, C.H., Connelly, A.: Mrtrix3: A fast, flexible and open software framework for medical image processing and visualisation. Neuroimage **202**, 116137 (2019)

41. Tschumperle, D., Deriche, R.: Variational frameworks for dt-mri estimation, regularization and visualization. In: Proc. of the IEEE International Conf. on Computer Vision. pp. 116–121 (2003)

42. Van Essen, D.C., Ugurbil, K., Auerbach, E., Barch, D., Behrens, T.E., Bucholz, R., Chang, A., Chen, L., Corbetta, M., Curtiss, S.W., et al.: The human connectome project: a data acquisition perspective. Neuroimage **62**(4), 2222–2231 (2012)

43. Vercauteren, T., Pennec, X., Perchant, A., Ayache, N.: Diffeomorphic demons: Efficient non-parametric image registration. Neuroimage **45**(1), S61–S72 (2009)
44. Wang, F., C, V.B.: Non-rigid multi-modal image registration using cross-cumulative residual entropy. International Journal of Computer Vision **74**, 201–215 (2007)
45. Wang, Z., Vemuri, B.C., Chen, Y., Mareci, T.H.: A constrained variational principle for direct estimation and smoothing of the diffusion tensor field from complex dwi. IEEE Transactions on Medical Imaging **23**(8), 930–939 (2004)
46. Wasserman, A.G.: Equivariant differential topology. Topology **8**(2), 127–150 (1969)
47. Wasserthal, J., Neher, P., Maier-Hein, K.H.: Tractseg-fast and accurate white matter tract segmentation. NeuroImage **183**, 239–253 (2018)
48. Weiler, M.: Equivariant and Coordinate Independent Convolutional Networks. Phd thesis, University of Amsterdam (2023)
49. Weiler, M., Geiger, M., Welling, M., Boomsma, W., Cohen, T.S.: 3d steerable cnns: Learning rotationally equivariant features in volumetric data. Advances in Neural Information Processing Systems **31** (2018)
50. Yang, X., Kwitt, R., Styner, M., Niethammer, M.: Quicksilver: Fast predictive image registration–a deep learning approach. NeuroImage **158**, 378–396 (2017)
51. Zhang, F., Wells, W.M., O'Donnell, L.J.: Deep diffusion mri registration (ddmreg): a deep learning method for diffusion mri registration. IEEE transactions on medical imaging **41**(6), 1454–1467 (2021)
52. Zhang, H., Yushkevich, P.A., Alexander, D.C., Gee, J.C.: Deformable registration of diffusion tensor mr images with explicit orientation optimization. Medical image analysis **10**(5), 764–785 (2006)
53. Zhang, P., Niethammer, M., Shen, D., Yap, P.T.: Large deformation diffeomorphic registration of diffusion-weighted imaging data. Medical image analysis **18**(8), 1290–1298 (2014)
54. Zhdanov, M., Hoffmann, N., Cesa, G.: Implicit convolutional kernels for steerable cnns. Advances in Neural Information Processing Systems **36** (2024)
55. Özarslan, E., Shepherd, T.M., Vemuri, B.C., Blackband, S.J., Mareci, T.H.: Resolution of complex tissue microarchitecture using the diffusion orientation transform (dot). Neuroimage (3), 1086–1103 (2005)